PHYSICAL REVIEW E **90**, 011102(R) (2014)

Reduced instability growth with high-adiabat high-foot implosions at the National Ignition Facility

D. T. Casey,[1] V. A. Smalyuk,[1] K. S. Raman,[1] J. L. Peterson,[1] L. Berzak Hopkins,[1] D. A. Callahan,[1] D. S. Clark,[1] E. L. Dewald,[1] T. R. Dittrich,[1] S. W. Haan,[1] D. E. Hinkel,[1] D. Hoover,[2] O. A. Hurricane,[1] J. J. Kroll,[1] O. L. Landen,[1] A. S. Moore,[3] A. Nikroo,[2] H.-S. Park,[1] B. A. Remington,[1] H. F. Robey,[1] J. R. Rygg,[1] J. D. Salmonson,[1] R. Tommasini,[1] and K. Widmann[1]

[1]*Lawrence Livermore National Laboratory, Livermore, California 94550, USA*

[2]*General Atomics, San Diego, California 92121, USA*

[3]*AWE Aldermaston, Reading, Berkshire RG7 4PR, United Kingdom*

(Received 20 February 2014; published 25 July 2014)

Hydrodynamic instabilities are a major obstacle in the quest to achieve ignition as they cause preexisting capsule defects to grow and ultimately quench the fusion burn in experiments at the National Ignition Facility. Unstable growth at the ablation front has been dramatically reduced in implosions with "high-foot" drives as measured using x-ray radiography of modulations at the most dangerous wavelengths (Legendre mode numbers of 30–90). These growth reductions have helped to improve the performance of layered DT implosions reported by O. A. Hurricane *et al.* [Nature (London) **506**, 343 (2014)], when compared to previous "low-foot" experiments, demonstrating the value of stabilizing ablation-front growth and providing directions for future ignition designs.

DOI: 10.1103/PhysRevE.90.011102 PACS number(s): 52.57.Fg, 52.70.La, 52.35.Py

In inertial confinement fusion (ICF), capsules containing deuterium-tritium (DT) fuel are imploded to high densities and temperatures with the aim of producing the conditions necessary for thermonuclear fusion [1]. In the indirect-drive scheme, lasers irradiate the inside of a gold hohlraum, producing x rays that then drive a capsule implosion. These x rays heat and ablate the capsule material outward, sending the remaining unablated mass, including a shell of cryogenically frozen DT fuel, imploding inward via momentum conservation. The imploding DT shell and remaining ablator then stagnate upon and heat a low density, gas-filled hot spot. Widely considered one of the grand challenges of modern science, achieving ignition and sustainable fusion burn of the fuel remains elusive [2,3]. Early in ICF research [3], it was realized that hydrodynamic instabilities and mix play a critical role in implosion performance degradation. Drive asymmetries and surface imperfections are amplified by hydrodynamic instabilities during the implosion, resulting in a distorted shell with reduced hot-spot temperature, pressure, and compression. Figure 1(a) illustrates the in-flight growth of seeds during the implosion and the resulting distortion to the hot spot with the ice ablator interface in green and a 1 keV temperature isosurface in red [4]. Much research has been devoted to the quantitative understanding of hydrodynamic instabilities in ICF implosions [1,5–9], resulting in sophisticated computer simulations and theoretical models to predict the consequences of the instabilities. These tools were used to design ignition experiments for the National Ignition Campaign (NIC) [10], conducted between 2009 and 2012, on the recently constructed 1.8 MJ laser at the National Ignition Facility (NIF) [11]. In these experiments, record compressions with fuel areal densities of $\sim$1.3 g/cm^2 have been achieved at fuel velocities of $\sim$320 km/s [12]. While these two key performance parameters were close to the goals of the ignition point design, the neutron yield performance was ten times lower than clean (no mix) one-dimensional (1D) simulations and four times less than that required by the point design [12,13]. Yet, understanding what led to this degraded performance has been elusive. This Rapid Communication provides direct experimental measurements of the growth at the ablation front as a function of mode and time for two different drives. Most importantly, here we show that we can sensitively change the ablation-front instability level and measure it at the onset, before stagnation where it is much harder to diagnose. This capability in our implosion tuning process will allow us to more rapidly improve NIF capsule performance and move toward higher yield implosions.

The implosion process is Rayleigh-Taylor (RT) unstable [1,5,14–17] during the acceleration phase because the ablating plasma pushes on the higher density unablated shell, satisfying the unstable condition $\nabla P \cdot \nabla \rho < 0$ (∇P and $\nabla \rho$ are the pressure and density gradients, respectively) [6,15]. The RT instability grows exponentially in time according to $\eta(t)/\eta_0 \approx e^{\gamma t}$ while in the linear regime ($\eta(t) \lesssim \lambda/2\pi$) [6], where η is a perturbation spatial amplitude, η_0 is the amplitude at $t = 0$, and λ is the perturbation wavelength. The growth rate [1,16] is approximately expressed by

$$\gamma = a_\gamma \sqrt{\frac{kg}{1+kL}} - \beta_\gamma k V_a, \tag{1}$$

where $k = 2\pi/\lambda$ is the perturbation wave number, g is the acceleration, $L = \rho/\nabla\rho$ is the density gradient scale length at the ablation front [16], and V_a is the ablation velocity or the mass ablation rate ($\dot{m}$) divided by the ablator density ($V_a = \dot{m}/\rho$) [1]. Here, a_γ and β_γ are functions of the dimensionless Froude number ($\mathrm{Fr} = V_a^2/gL$) and thermal conductivity [16]. The ignition target point design [18] was optimized for performance and stability considerations using a low-adiabat (α) or "low-foot" drive to reach high compression with a plastic CH ablator with roughness requirements designed to mitigate damage from RT growth. Here α can be defined as $\alpha = P/P_{\mathrm{cold}}$, where P_{cold} is the minimum pressure at 1000 g/cm^3 from the DT equation of state (EOS) [18]. However, experiments [13,19,20] have shown that instability growth and mix are much worse for the point design than originally predicted for reasons that are not yet fully understood.

Dittrich *et al.* hypothesized that this anomalous mix and the subsequent failure of the low-foot platform to achieve ignition may be a result of an overestimate of ablative stabilization in

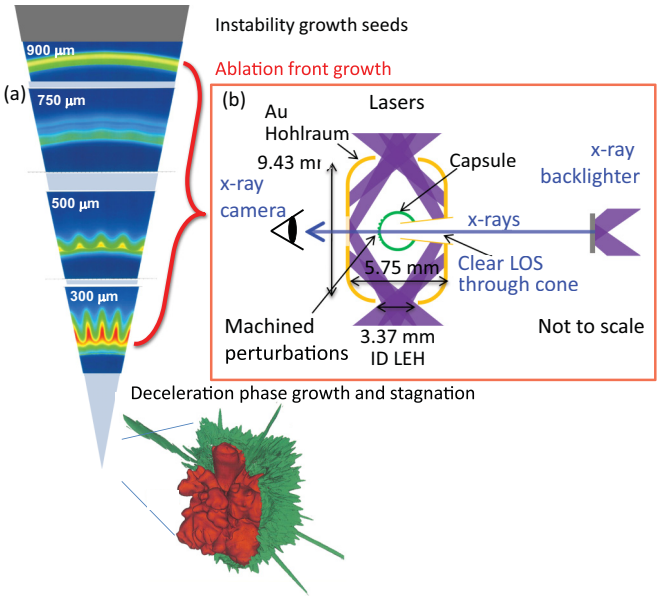

FIG. 1. (Color online) (a) Schematic diagram of instability growth at several different radii showing density contours from HYDRA simulations. Also shown is a simulated stagnated hot spot showing the consequences of instability growth. (b) Schematic of an indirectly driven hydrogrowth radiography target. The capsules are machined with sinusoidal perturbations and backlit using a V foil x-ray backlighter.

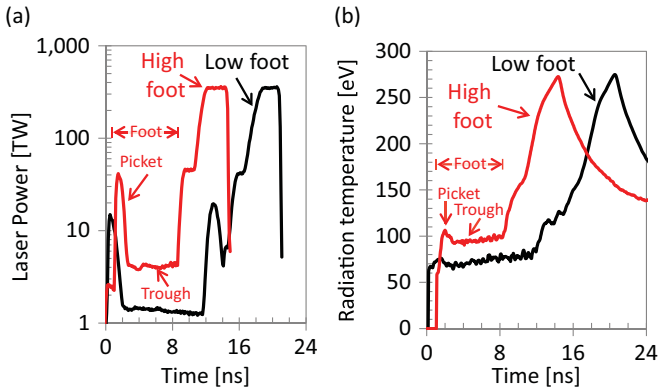

FIG. 2. (Color online) (a) Laser pulse shape and (b) radiation drive temperature measured on two NIF shots, one shot with the low-adiabat (or low-foot, black curve) and the other with the high-adiabat (or high-foot, red curve) drive.

calculations and simulations [21]. The developed hydrogrowth radiography platform [22,23], illustrated in Fig. 1(b), was used to measure growth for the low- and high-foot drives during the ablative phase. This platform uses the ignition target design [18] for the hohlraum and the Si-doped CH ablator. The target is similar to actual ignition targets except that the capsule uses a surrogate CH payload to replace the cryogenic DT ice layer and the diagnostic uses an Au cone penetrating one side of the capsule. The capsule has an outer radius of 1120 μm with a total shell thickness of 206 μm. The plastic ablator is doped with three layers of graded Si at 2, 4, and 2 at. %. The inner plastic layer contains a mass-equivalent payload of undoped plastic ~14 μm for a typical cryogenic ice layer (momentum balanced to achieve the same implosion velocity) accounting for the density of CH at 1.06 g/cm^3 (at 32 K) and the solid DT density of 0.255 g/cm^3 (at 20 K). The Au hohlraum is 5.75 mm inner diameter by 9.43 mm tall (inside), with a laser entrance hole 3.1 mm in diameter, and is filled with He.

Three capsule types with preimposed sinusoidal perturbations were used. The first was machined to have an initial perturbation wavelength of 240 μm and 1.7 μm amplitude (peak to valley) for a Legendre polynomial mode number of $\ell = 30$, where $\ell = 2\pi R/\lambda = kR$. The second had 120 μm wavelength and 3.4 μm amplitude for $\ell = 60$. The third had both 120 and 80 μm wavelengths, corresponding to $\ell = 60$ and 90, placed side by side with amplitudes of 0.5 and 0.6 μm, respectively.

A 12.5 μm thick V backlighter [24] is used to radiographically observe the perturbation amplitudes in flight as a function of time. The V foil is irradiated using eight NIF laser beams focused to an intensity of ~5 $\times$ 10^{14} W/cm^2. In conjunction with x-ray filtering, this produces a nearly monochromatic ~5.4 keV x-ray source from a combination of mostly V He-α and Ly-α that lasts about ~3 ns.

The high-foot experiments have demonstrated a significantly higher implosion performance [21,25,26], much closer to clean 1D simulations, by delivering higher entropy to the fuel and ablator. The entropy, or equivalently, α, was increased by raising the intensity of the initial picket and trough (collectively, the foot) of the laser pulse [see Fig. 2(a)]. The corresponding measured radiation temperatures are shown in Fig. 2(b); both drives reach a peak T_r of 270–280 eV. The high-foot drive is predicted to have significantly reduced ablation-front growth, hypothesized as a primary reason for the enhanced performance [21,25,26]. To test the effectiveness of the high-foot design in reducing ablation-front growth, experiments were conducted to directly measure single-mode, linear-regime, ablation-front growth for both the low- and high-foot drives. These experiments used laser pulse shapes [shown in Fig. 2(a)] that were matched to a low-foot cryogenic DT shot (~350 TW peak power) and a high-foot cryogenic DT shot (also ~350 TW). The measured hohlraum radiation temperatures, obtained by the Dante diagnostic [27], are shown in Fig. 2(b).

Figures 3(a) and 3(c) show slit image radiographs of modulation growth captured on an x-ray imager using the low-foot and high-foot pulses, respectively. The images are timed to show the capsule at approximately the same in-flight radii. Distinct differences in contrast are observed due to reduced growth for $\ell = 60$ with the high-foot drive. More dramatically, $\ell = 90$ shows very little growth for the high-foot drive [consistent with the predictions shown in Fig. 5(b)] because it is near a change in phase ("growth-factor zero crossing") due to amplitude oscillation during the Richtmyer-Meshkov (RM) phase, or shock transit phase [28,29], and because the density scale length and ablative stabilization effects are stronger.

Figure 4 shows the measured modulation amplitude in optical depth (OD), obtained using the low-foot and high-foot drives, during the early phase of the implosion, plotted as a function of wavelength for $\ell = 60$ [Figs. 4(a) and 4(b)] and

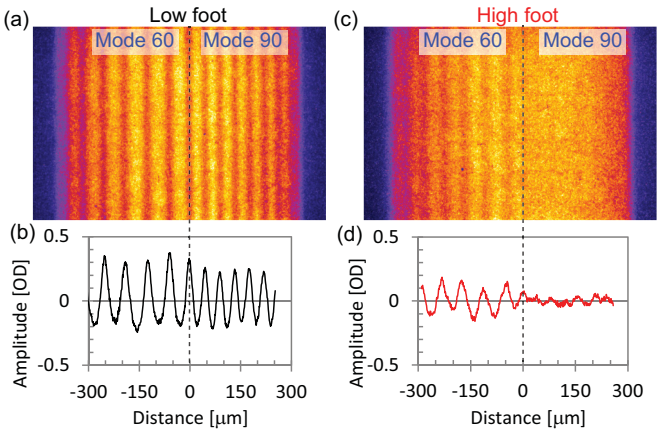

FIG. 3. (Color online) (a) Slit image radiograph of side-by-side, preimposed, single-mode ripples of $\ell = 60$ and 90, for the low-foot pulse at 20.6 ns, which corresponds to a radius of ~613 μm. (b) Horizontal line-out in optical depth of the slit image shown in (a). (c) Also shown is a slit image radiograph at 14.8 ns, driven with the high-foot pulse, which corresponds to a radius of ~600 μm for the same side-by-side modes. (d) Horizontal line-out in optical depth of the slit image shown in (c).

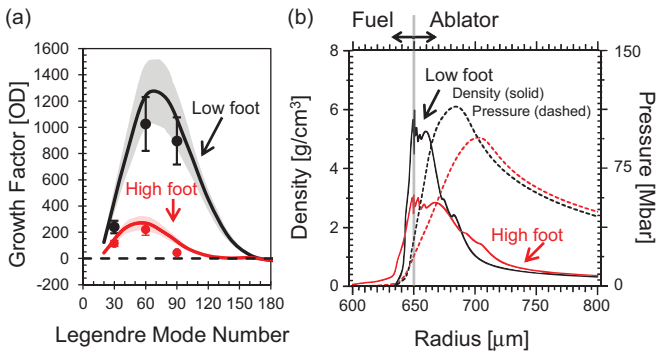

FIG. 5. (Color online) (a) Measure and simulated OD growth factors for low-foot (black) and high-foot (red) drives, plotted as a function of mode number at an imploded radius of ~630 μm. (b) Density (solid curves) and pressure (dashed curves) profiles simulated for layered DT implosions driven by the low-foot (black curve) and the high-foot (red curve) drives using the code HYDRA [34]. The ablation front is near the point of maximum pressure. The simulated profiles clearly show a longer ablation-front scale length, a lower peak density, and a lower in-flight aspect ratio for the high-foot drive, all properties that enhance stability.

$\ell = 90$ [Fig. 4(c)]. Here, $\mathrm{OD} = -\ln(I/I_0) = \int \kappa \delta \rho d R$, where the opacity ($\kappa$) is for an x-ray energy of 5.4 keV. Note also that the initial perturbation OD amplitude of the targets used in Figs. 4(a)–4(c) are 2.7×10^{-3}, 4.0×10^{-4}, and 4.7×10^{-4}, respectively [30]. The fundamental harmonic amplitude is obtained using a Fourier analysis of the central few peaks shown in Figs. 3(b) and 3(d). The growth is plotted as a function of the measured wavelength, since the wavelength of the perturbation is directly related to the implosion radial trajectory via $R(t) = \lambda(t) l/(2\pi)$. The corresponding radius is indicated on the top axis. As the capsule implodes, both the radius and the perturbation wavelength are reduced. The result demonstrates a distinct reduction (~2 times smaller) in the growth using the high-foot drive at $\ell = 60$ and an order of magnitude smaller growth at $\ell = 90$.

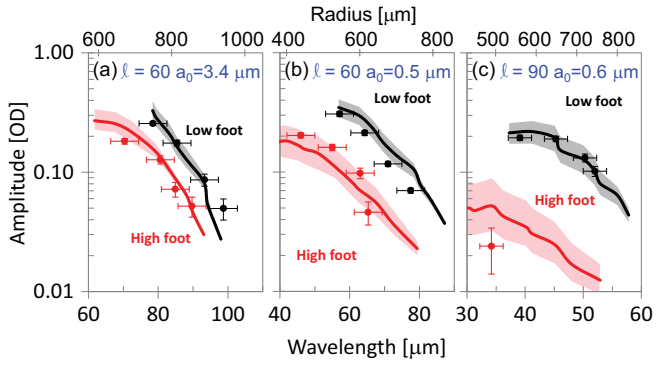

FIG. 4. (Color online) (a) Optical depth (OD) modulation amplitude of the fundamental harmonic as a function of wavelength (the top axis shows the equivalent radius) for $\ell = 60$ for both the low-foot (black) and high-foot (red) drives observed with a 3.4 μm deep (peak-to-valley) modulation initial amplitude. The curves are HYDRA simulations of OD amplitude, while the data are represented by symbols. The shaded bands are included on simulations (solid curves) to illustrate the sensitivity to uncertainties in the drive and the simulation methodology. (b) OD amplitude for $\ell = 60$ with 0.5 μm initial amplitudes. (c) OD amplitude for $\ell = 90$ with 0.6 μm initial amplitudes.

Figure 4 also shows the simulated OD due to instability growth [23], including the diagnostic resolution, compared to the observations. The sources of uncertainty in the growth calculations include uncertainties in the drive and in the initial amplitude as it varies across the imposed perturbation. In particular, the high energy (>1.8 keV), or M-band, portion of the drive is expected to be a dominant source of uncertainty [18], since the mean free path of the drive x rays determines the ablation-front scale length [31] and preheating by the high energy photons affects the density of the unablated CH. However, recent experiments have helped to reduce uncertainties in the drive and spectrum seen by the capsule [32,33]. The simulations, shown in Fig. 4, include bands of uncertainty that correspond to ±33% in the M-band fraction, which is an estimate of the remaining growth uncertainty. The comparison shows good agreement between simulation and data and provides a quantitative test of the simulations using these two different drives, at $\ell = 60$ and 90, within this experimental window.

Figure 5(a) shows the experimentally determined growth factors, defined as final over initial perturbation amplitude in OD, plotted as a function of mode number and compared with 2D HYDRA simulations at radii of ~630 μm. The simulations use the opacity at the backlighter energy to compare the growth-factor amplitude in optical depth with the measurement. Here the reduction of the modulation amplitude due to experimental resolution was removed. The results clearly indicate that the high-foot drive is more stable when compared to the low-foot drive and that the stabilizing effects are well reproduced by HYDRA. The growth is stabilized by the ablation process through the density gradient scale

length and ablation velocity. Reduced compression of the high-foot's higher α ablator (as established during the foot of the drive), in the main acceleration phase, produces a lower ablator density, an increased ablation velocity, and an increased density gradient scale length. The higher α and lower ablator density also result in a longer mean free path for the drive x rays at the ablation front, which is partly responsible for increasing the ablation-front scale length (gentler density slope) [31], as illustrated in Fig. 5(b) with a comparison of the density profiles calculated using HYDRA. The times have been chosen to compare the two density profiles when the DT-fuel/CH-ablator interface is at 650 μm for both drives ($\sim$1.4 times smaller than the initial interface radius). The simulated profiles clearly show a longer ablation-front scale length, and a lower peak density. This also results in a lower in-flight aspect ratio by $\sim$1.5–2 for the high-foot drive, which further enhances stability [21,25,26]. The hypothesis that anomalous ablation-front growth was responsible for the performance degradation of the low-foot drive by Dittrich *et al.* is shown by these results to be unlikely. Furthermore, the predictability of the high-foot growth benchmarks the simulation of the stabilizing effects of ablation (previously called into question), providing both a path to reducing growth and raising confidence in more robust platforms to achieve ignition.

In summary, a 350 TW high-adiabat (high-foot) drive stabilizes hydrodynamic instability when compared to a similar power low-adiabat (low-foot) drive. Instability growth calculations do well at reproducing the measured data up to convergence $R_0/R \sim 2$ when the initial seeds are well known. This suggests that unknown seeds, such as perturbations from the capsule support tent [35], may be a significant factor in the performance degradation of the low-foot implosions. This picture is supported by recent high resolution three-dimensional (3D) HYDRA simulations including different models for the tent perturbation that better reproduce the performance of some NIC implosions [4]. It is also possible that seeds at other interfaces (e.g., fuel/ablator interface), from defects inside the CH plastic, and growth at higher convergence could play an important role in reducing implosion performance. To study these issues, future experiments are proposed to observe the 3D broadband growth from unperturbed capsules up to $R_0/R \sim 5$, similar to previous experiments performed on OMEGA [36].

The improved performance of the high-foot drives in cryogenic layered DT implosions described elsewhere [21,25,26], along with the reduced hydrodynamic growth demonstrated herein, underscore the value of mitigating instability growth in NIF ignition experiments. More specifically, by raising the foot of the radiation drive, the high-foot drive reduced instability growth by shifting the region of positive growth to a lower mode number, increasing the ablator density scale length, increasing the ablation velocity, and decreasing the in-flight aspect ratio [21,25,26,37]. These results will help inform future experiments designed to achieve thermonuclear ignition. For example, previous experiments in direct drive have stabilized instability growth using an adiabat shaping technique with unsupported decaying shocks driven by laser pickets [38], raising the outer ablator adiabat, while decaying to a lower adiabat in the ice layer. Now having demonstrated that instability growth can be controlled using the high-foot drive, this adiabat shaping technique is under development for an indirect drive at NIF to increase the final fuel compression while stabilizing the RT growth at the ablation front.

The authors thank the NIF operations staff who supported this work. This work was performed under the auspices of the US Department of Energy by Lawrence Livermore National Laboratory under Contract No. DE-AC52-07NA27344.

[1] J. D. Lindl, P. Amendt, R. L. Berger, S. G. Glendinning, S. H. Glenzer, S. W. Haan, R. L. Kauffman, O. L. Landen, and L. J. Suter, Phys. Plasmas **11**, 339 (2004).
[2] J. H. Nuckolls, J. Phys.: Conf. Ser. **244**, 012007 (2010).
[3] J. Nuckolls, L. Wood, A. Thiessen, and G. Zimmerman, Nature (London) **239**, 139 (1972).
[4] D. Clark *et al.*, IOP J. Phys. Conf. Ser. (to be published).
[5] J. D. Kilkenny *et al.*, Phys. Plasmas **1**, 1379 (1994).
[6] S. Atzeni and J. Meyer-ter-Vehn, *The Physics of Inertial Fusion*, International Series of Monographs on Physics No. 125 (Oxford University Press, Oxford, UK, 2004).
[7] V. A. Smalyuk, Phys. Scr. **86**, 058204 (2012).
[8] T. J. B. Collins, J. P. Knauer, R. Betti, T. R. Boehly, J. A. Delettrez, V. N. Goncharov, D. D. Meyerhofer, P. W. McKenty, S. Skupsky, and R. P. J. Town, Phys. Plasmas **11**, 1569 (2004).
[9] K. Otani, K. Shigemori, T. Sakaiya, S. Fujioka, A. Sunahara, M. Nakai, H. Shiraga, H. Azechi, and K. Mima, Phys. Plasmas **14**, 122702 (2007).
[10] M. J. Edwards *et al.*, Phys. Plasmas **18**, 051003 (2011).
[11] E. I. Moses, J. Phys.: Conf. Ser. **112**, 012003 (2008).
[12] V. A. Smalyuk *et al.*, Phys. Rev. Lett. **111**, 215001 (2013).
[13] M. J. Edwards *et al.*, Phys. Plasmas **20**, 070501 (2013).
[14] B. A. Remington, S. W. Haan, S. G. Glendinning, J. D. Kilkenny, D. H. Munro, and R. J. Wallace, Phys. Rev. Lett. **67**, 3259 (1991).
[15] R. Betti, V. N. Goncharov, R. L. McCrory, P. Sorotokin, and C. P. Verdon, Phys. Plasmas **3**, 2122 (1996).
[16] R. Betti, V. N. Goncharov, R. L. McCrory, and C. P. Verdon, Phys. Plasmas **5**, 1446 (1998).
[17] S. G. Glendinning *et al.*, Phys. Plasmas **7**, 2033 (2000).
[18] S. W. Haan *et al.*, Phys. Plasmas **18**, 051001 (2011).
[19] S. P. Regan *et al.*, Phys. Rev. Lett. **111**, 045001 (2013).
[20] T. Ma *et al.*, Phys. Rev. Lett. **111**, 085004 (2013).
[21] T. R. Dittrich *et al.*, Phys. Rev. Lett. **112**, 055002 (2014).
[22] V. A. Smalyuk *et al.*, Phys. Rev. Lett. **112**, 185003 (2014).
[23] K. Raman *et al.*, Phys. Plasmas **21**, 072710 (2014).
[24] C. M. Huntington, C. M. Krauland, C. C. Kuranz, R. P. Drake, H.-S. Park, D. H. Kalantar, B. R. Maddox, B. A. Remington, and J. Kline, Rev. Sci. Instrum. **81**, 10E536 (2010).
[25] H. S. Park *et al.*, Phys. Rev. Lett. **112**, 055001 (2014).
[26] O. A. Hurricane *et al.*, Nature (London) **506**, 343 (2014).
[27] E. L. Dewald *et al.*, Rev. Sci. Instrum. **75**, 3759 (2004).
[28] V. N. Goncharov, Phys. Rev. Lett. **82**, 2091 (1999).

[29] L. Peterson *et al.*, Phys. Plasmas (to be published).
[30] The initial OD comes from the machined outer CH on the capsule surface. However, much of the observed optical depth during the experiment comes from compressed Si doped CH at the ablation front.
[31] S. V. Weber, B. A. Remington, S. W. Haan, B. G. Wilson, and J. K. Nash, Phys. Plasmas **1**, 3652 (1994).
[32] S. A. MacLaren *et al.*, Phys. Rev. Lett. **112**, 105003 (2014).
[33] M. Schneider *et al.*, IOP J. Phys. Conf. Ser. (to be published).
[34] M. M. Marinak, G. D. Kerbel, N. A. Gentile, O. Jones, D. Munro, S. Pollaine, T. R. Dittrich, and S. W. Haan, Phys. Plasmas **8**, 2275 (2001).
[35] S. R. Nagel (unpublished).
[36] V. A. Smalyuk, S. X. Hu, J. D. Hager, J. A. Delettrez, D. D. Meyerhofer, T. C. Sangster, and D. Shvarts, Phys. Plasmas **16**, 112701 (2009).
[37] R. Tommasini *et al.* (unpublished).
[38] J. P. Knauer *et al.*, Phys. Plasmas **12**, 056306 (2005).